A NUMERICAL APPROACH TO PREDICT SULPHUR DIOXIDE EMISSIONS DURING SWITCHGRASS COMBUSTION

Bernhard Peters[*], Joanna Smuła-Ostaszewska

Université du Luxembourg, 6, rue Coudenhove-Kalergi, L-1359 Luxembourg, Luxembourg

The demand for a net reduction of carbon dioxide and restrictions on energy efficiency make thermal conversion of biomass a very attractive alternative for energy production. However, sulphur dioxide emissions are of major environmental concern and may lead to an increased corrosion rate of boilers in the absence of sulfatation reactions. Therefore, the objective of the present study is to evaluate the kinetics of formation of sulphur dioxide during switchgrass combustion. Experimental data that records the combustion process and the emission formation versus time, carried out by the National Renewable Energy Institute in Colorado (US), was used to evaluate the kinetic data.

The combustion of switchgrass is described sufficiently accurate by the Discrete Particle Method (DPM). It predicts all major processes such as heating-up, pyrolysis, combustion of switchgrass by solving the differential conservation equations for mass and energy. The formation reactions of sulphur dioxide are approximated by an Arrhenius-like expression including a pre-exponential factor and an activation energy. Thus, the results predicted by the Discrete Particle Method were compared to measurements and the kinetic parameters were subsequently corrected by the least square method until the deviation between measurements and predictions was minimised. The determined kinetic data yielded good agreement between experimental data and predictions.

Keywords: biomass combustion, sulphur dioxide emissions, kinetic parameters, optimisation

1. INTRODUCTION

A continuous effort to reduce the net emission of carbon dioxide (CO_2) makes renewable fuels such as biomass an attractive alternative for energy production. However, conditions for both combustion and operation of plants impose further challenges (Ściążko et al., 2007) because the composition of biomass differs considerably from coal. Economic aspects of co-combustion of coal and biomass in Poland were analysed in the work of Ericsson (2007). The author compared advantages and weaknesses of co-combustion in large and small power plants. The study indicated the effectiveness of total emission reduction by co-firing of coal and biomass, whereas SO_2-emission reduction was significant only in small plants, which did not apply any fuel desulphurisation. The combustion of biomass results in a significant formation of acidic pollutants, high mass loading of aerosols in the flue gas and agglomeration of these aerosols on heat-transfer surfaces (Aho and Silvennoinen, 2004; Dayton et al., 1995; Ściążko et al., 2007; Knudsen et al., 2004a; Lang et al., 2006; Michelsen et al., 1998; Misra et al., 1993; Ściążko et al., 2007; Van Lith et al., 2006; Wiinikka et al., 2007). Among these pollutants are sulphur components that contribute significantly to the above-mentioned risks (Knudsen et al., 2004b; Knudsen et al., 2005; Lang et al., 2006; Wiinikka et al., 2007) . Comparison of the amount of emissions, such as CO, NO_x and SO_2, produced by combustion of different sorts of biomass can be found in works of Koyuncu and Pinar (2007), of Verma et al. (2011) and of Roy and Corscadden
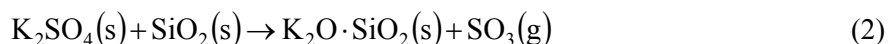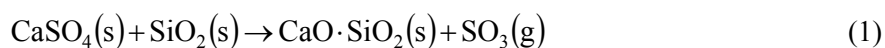
---

*Corresponding author, e-mail: bernhard.peters@uni.lu

(2012). The authors reported properties of particular types of biomass, which are applied as fuels in domestic stoves or boilers. Observations presented by Knudsen et al. (2004a) allowed to determine that 30 - 55% sulphur was transformed into sulphur dioxide (SO2) and was released below 500ºC during combustion of annual biomass. Moreover, samples rich in potassium and calcium, but low in silicon, showed only a slight increase of sulphur release to the gas phase with a further increase of combustion temperature. However, the release of sulphur increases abruptly above 700-800ºC for biomass with a high silicon content. Further investigations of Knudsen et al. (2004b; 2005) on wheat straw and beech wood showed that sulphur dioxide captured by secondary reactions during char burnout was retained in the bottom ash. This process was most effective at about 600ºC, where approximately 85% of released sulphur dioxide was retained.

Van Lith et al. (2006) found that sulphur was released through evaporation of sulphates or as sulphur dioxide (SO_2) for woody biomass. A maximum release rate close to 100% was observed at ~1150ºC. They described potential reaction paths and their chemical analysis included scanning electron microscopy and predictions for the equilibrium state.

Wiinikka et al. (2007) investigated the formation of high temperature aerosols during fixed bed combustion dependent on the ash composition of the fuel. It was observed, that particles of alkali sulphates (K_2SO_4 and Na_2SO_4) and chlorides (KCl and NaCl) were formed from the inorganic vapour during cooling of the flue gas. The initial alkali concentration and the alkali to silicon ratio (K+Na)/Si influenced the amount of vaporised aerosols. Their total concentration in the gas phase was correlated to the amount of alkali sulphates and chlorides volatilised from the fuel bed.

In order to increase retention of sulphur in the bottom ash Lang et al. (2006) added a sulphur-binding calcium-sorbent to annual biomass. The complex and temperature dependent interactions between the adsorbent and the components of the fuel such as sulphur, potassium and silicon affected the retention of sulphur to a large amount. They suggested that at temperatures of ~800ºC reactions between silicon and sulphates of potassium and calcium according to

$$CaSO_4(s) + SiO_2(s) \rightarrow CaO \cdot SiO_2(s) + SO_3(g) \tag{1}$$

$$K_2SO_4(s) + SiO_2(s) \rightarrow K_2O \cdot SiO_2(s) + SO_3(g) \tag{2}$$

contribute to an increased release of sulphur oxides instead of retaining sulphur as sulphates.

At temperatures between 800 and 1100ºC, sulphation reactions became dominant, but were limited by the low fraction of sulphur that remained in a char after the initial devolatilisation phase. Their results showed that ~25 - 35% of sulphur dioxide could be retained in the ash at 1100ºC, when calcium-sorbents were added. Lang et al. (2006) suggested also that an optimum desulphurisation effectiveness would be obtained if the atomic ratio $(Ca + 1/2K)_{total}/Si_{total}$, which they referred to as SRI factor would be greater than 2 or even closer to 4.

Based on the above-mentioned review of literature (Knudsen et al., 2004a; Lang et al., 2006; Van Lith et al., 2006; Zheng et al., 2007) the following figure (Fig. 1) for transformation of sulphur during thermal treatment of biomass was derived.

Sulphur occurs in biomass as both organic bound sulphur (Organic-S) and inorganic salts (Inorganic-S) that follow different reactions paths.

1.1. Organically bound sulphur

During devolatilisation and temperatures below ~500ºC, organic sulphur follows three reaction paths that yield gaseous sulphur, hydrogen sulphide or sulphur dioxide. These products may undergo further reactions during which sulphur attaches to the char matrix for temperatures above ~600ºC.

Furthermore, hydrogen sulphide may form alkali sulphides that in conjunction with char-bound sulphur constitute the major products during pyrolysis and gasification of biomass. In the presence of oxygen char-bound sulphur is converted to sulphur dioxide (Knudsen et al., 2004a; Lang et al., 2006; Wiinikka et al., 2007; Zheng et al., 2007) that may form sulphates in the presence of alkali metals.
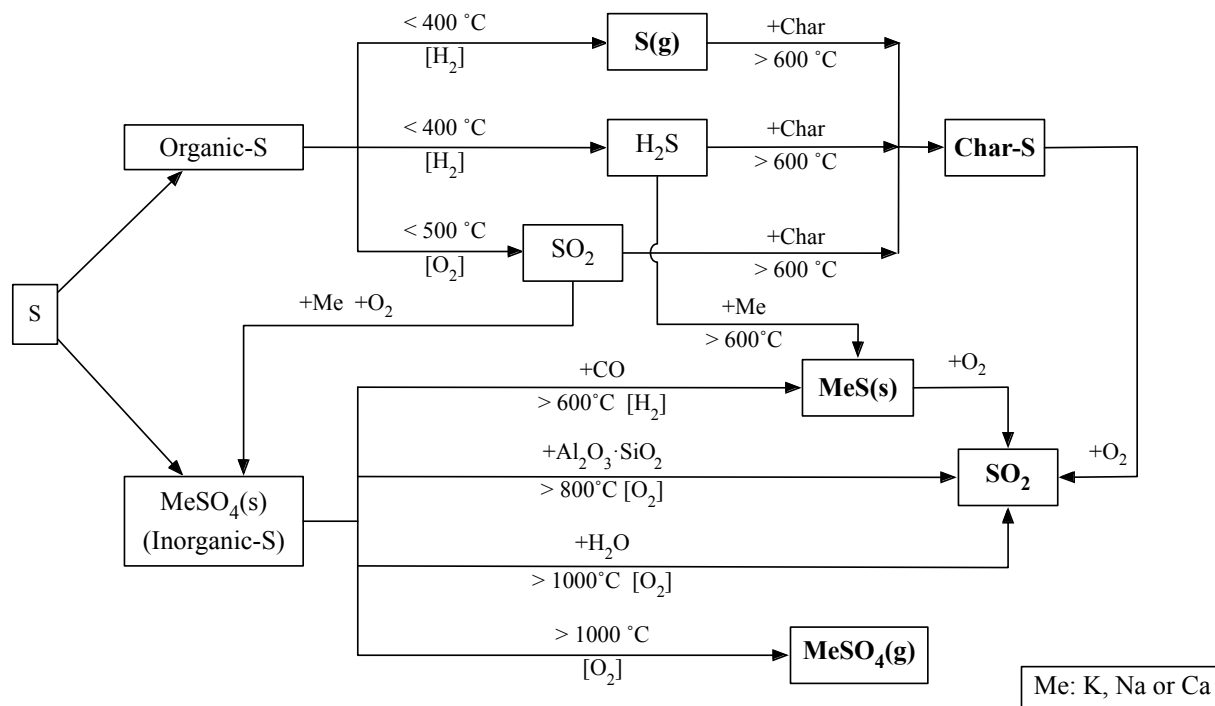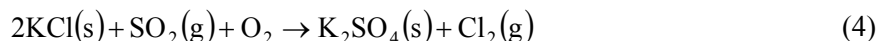

Fig. 1. Simplified scheme of sulphur transformations under reduction/oxidising conditions
(bold-faced species indicate major products)

1.2. Inorganically bound sulphur

Alkali salts of sulphur stemming also from the decomposition of organically bound sulphur usually undergo different reactions at elevated temperatures above ~600ºC after the devolatilisation phase. At a temperature higher than ~600ºC carbon monoxide reduces sulphates to alkali sulphites, which may be oxidised by oxygen to sulphur dioxide. Alkali sulphates are reduced to sulphur dioxide in an oxidising environment in the presence of either aluminium silicates (T > 800ºC) or water vapour (T > 1000ºC). Furthermore, sulphates may evaporate from biomass with low contents of silicates at temperatures higher than 1000ºC (Knudsen et al., 2004a; Lang et al., 2006; Wiinikka et al., 2007; Zheng et al., 2007). Although sulphur causes emission problems, it is accompanied by a positive side-effect due to the following reactions (Matsuda et al., 2005; Michelsen et al., 1998; Nielsen et al., 2000; Ściążko et al., 2007):

$$2KCl(s) + SO_2(g) + \tfrac{1}{2}O_2 + H_2O \rightarrow K_2SO_4(s) + 2HCl(g) \qquad (3)$$

or in absence of water vapour:

$$2KCl(s) + SO_2(g) + O_2 \rightarrow K_2SO_4(s) + Cl_2(g) \qquad (4)$$

As an advantage hydrogen chloride and chlorine formed by reaction 3 and 4 respectively, do not condensate on boiler surfaces contrary to alkali chlorides (Michelsen et al. 1998; Aho and Ferrer 2005). However, a protective effect of these reactions occurs for a fuel molar ratio S/Cl not smaller than 2.0 and under oxidising conditions (Ściążko et al. 2007). Comprehensive discussions of sulphation of chlorides in boiler deposits may be found in the following articles (Aho and Ferrer, 2005; Michelsen et al., 1998; Nielsen et al. 2000; Ściążko et al., 2007).

Co-firing of different biomass fuels or coal usually does not lead to reduced sulphur emissions because inherently existing potassium chloride has a higher reactivity with aluminium-silicates than sulphur compounds (Aho and Ferrer, 2005; Aho and Silvennoinen, 2004; Zheng et al., 2007). Therefore, chlorides are reduced by co-firing straw with coals having high levels of Si and Al instead of high sulphur content coals or an addition of significant amounts of sulphur dioxide. Zheng et al. (2007) suggested that known molar ratios of K/Si, K/(S+Si), S/Cl and Ca/Si could be used to predict co-combustion products of potassium chloride and sulphate, respectively. Their results of potassium chloride and sulphate concentrations in the fly ash showed reasonable agreement with full-scale plant-data presented in literature.

Kinetics of thermal treatment of biomass, which included sulphur dioxide as a product of the process, was presented in literature recently. Namely the kinetics of combustion of grape pomace blended with Pyrenean oak was studied by Miranda et al. (2012). However, the authors did not specify directly chemical reactions, which take place during combustion and sulphur dioxide was mentioned as one of the products of that process. Besides, kinetics of combustion of hazelnut shell with lignite was conducted by Kulah (2010). The presented model of biofuel decomposition included sulphur retention by instantaneous calcination of limestone followed by sulphation reaction.

According to the best knowledge of the authors, data presented in literature never includes kinetic parameters of chemical reactions during biomass combustion forming sulphur dioxide emissions. Dayton et al. (1995) measured the evolution of emission of components during combustion of switchgrass. From these results kinetic data was derived to predict emission formation by the Discrete Particle Method (DPM).

2. EVALUATION OF CHEMICAL KINETICS

2.1. Analysis of experimental data

At first experimental data was analysed and processed. It involved time-dependent release of sulphur dioxide and a description of the properties of the switchgrass sample. Then, the Discrete Particle Method (DPM) was employed to describe both the combustion of switch grass and the release of sulphur dioxide. The obtained results were compared to experimental data and the kinetic parameters were corrected to minimise the deviation.

2.2. Analysis of sulphur dioxide release

The emission of sulphur dioxide at different ambient conditions during the combustion of switchgrass was investigated and reported by Dayton et al. (1995). They combusted ~40 mg of ground switchgrass placed in a boat in an electric clamshell furnace preheated up to ~1100ºC. A total gas flow rate of 4.4 l/min with an oxygen concentrations of 5, 10 or 20% flowed through the reactor which amounts to a residence time of ~0.1 s. Figure 2 depicts the gas temperature in the vicinity of the switchgrass sample. It was measured by a type-K thermocouple surrounded by a 0.5 mm diameter inconel sheath.

Sample gases were extracted from the reactor and subsequently analysed by molecular beam/mass spectrometry (MBMS). This yielded a complete mass spectrum of the combustion gas every 1.0 - 1.5 s. For a detailed description of the experimental set-up the reader is referred to the article of Dayton et al. (1995).
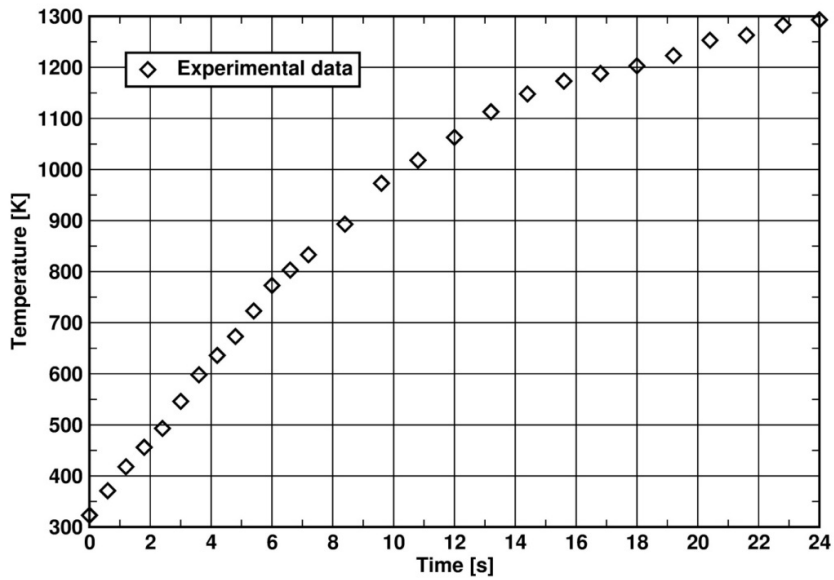
Fig. 2. Measured temperature profile during switchgrass combustion

The ion intensity measured by the molecular beam/mass spectrometry was converted into a concentration profile for sulphur dioxide. Since the intensity, I, is proportional to the concentration c_i, $(I \sim c_i)$, the instantaneous intensity can be written as

$$I = \gamma \cdot \dot{Q} \cdot c_i \tag{5}$$

with γ and $\dot{Q}$ being the constant of proportionality and the volumetric flow rate, respectively. The volumetric flow rate was constant, thus an integration of Eq. 5 between the times t_1 and t_2 yields the amount of released species i:

$$\int_{t1}^{t2} I dt = \gamma \cdot Q \int_{t1}^{t2} c_i dt = n_{tot} \tag{6}$$

where the integral represents the total number of moles n_{tot} released. Applying the above-mentioned relationships the measured intensity was converted to a concentration profile shown in Figure 3.
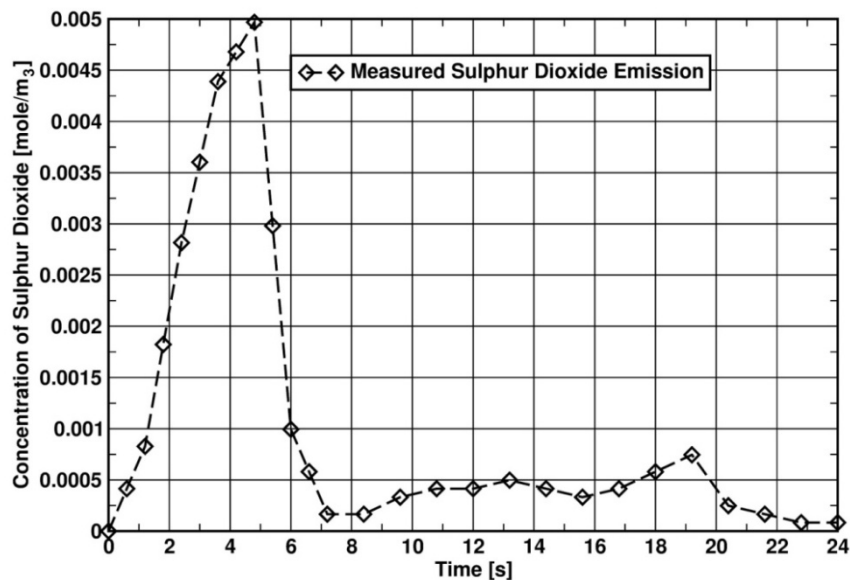
Fig. 3. Concentration of sulphur dioxide c_{SO2} released during combustion of ~40 mg of switchgrass in an atmosphere of 20% O_2 in He and a furnace temperature of 1100 ºC

Experimental data in Figure 3 suggest that the first peak of emitted sulphur dioxide occurs during pyrolysis while the following period of emissions takes place during combustion of the charred material.

As mentioned in the previous section sulphur dioxide is primarily formed from sulphur bound to char and the potassium sulphate according to the following conversion reactions:

$$S + O_2 \rightarrow SO_2 \tag{7}$$

$$K_2SO_4 + SiO_2 \rightarrow K_2O \cdot SiO_2(s) + SO_2 + \frac{1}{2}O_2 \tag{8}$$
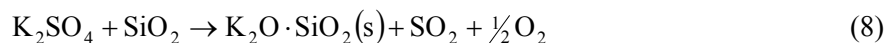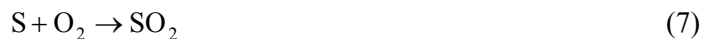
The former corresponds to a reaction that takes place at low temperatures up to 500 ºC, whereas the latter is predominantly restricted to higher temperatures above 800 ºC. This temperature dependence becomes apparent in Figure 3, in which sulphur dioxide is formed during two different periods that correspond to different temperature regions according to Figure 2. Thus, the respective areas of the profile represent the fraction of sulphur dioxide formed by the reactions defined by Eq. 7 and Eq. 8, respectively. Evaluation of the areas gives a ratio of 74:26 for sulphur dioxide formed by both reactions.

The analysis of switchgrass (Dayton et al., 1995) is shown in Table 1. The density of chopped switchgrass amounts to $\rho \sim 108$ kg/m^3 (McLaughlin et al., 1999).

Table 1. Proximate analysis for switchgrass

proximate	%wt dry basis
fixed carbon	16.22
volatile	79.19
ash	4.59
S	0.11

2.3. Properties of the packed bed of switchgrass

Approximately 40 mg of ground and loosely packed switchgrass was placed inside the furnace that resembled a packed bed of switchgrass particles. In order to represent all individual particle processes by a single particle, gradients concerning both temperature and reaction within the packed bed have to vanish which is comparable to a well stirred-reactor model (Peters, 1999). Therefore, Damköhler numbers for the ratio of reaction and heat generation time to a convective transport time were assessed. The used Damköhler numbers are

$$Da_1 = \frac{\dot{\omega}L}{v\rho_0} \tag{9}$$

$$Da_2 = \frac{\dot{\omega}QL}{v\rho c_p T} \tag{10}$$

where $\dot{\omega}$, L, v, Q, ρ, c_p and T denote a representative reaction rate, length scale, gas velocity, heat source due to conversion, density, specific heat capacity and temperature, respectively. The reactions rate $\dot{\omega}$ was assessed by the mass of switchgrass over the conversion time of 20 s, whereby the length scale was assumed to be the order of 10-2 m. The gas velocity was evaluated with ~0.4 m/s derived from the applied flow rate. The remaining material properties were taken as those of switchgrass, so that both Damköhler numbers were estimated as 10-2 and 10-5, respectively. Hence, these values

indicate homogeneous conditions throughout the packed bed with vanishing gradients similar to a well-stirred reactor (Peters,1999). Therefore, the behaviour of a single particle represents the over-all behaviour of the packed bed, and thus, predictions of a single particle describe the process with sufficient accuracy.

Although in the current application a simple lumped parameter model for thermally thin particles would suffice, the chosen approach treats both thermally thin and thick particles. This is reasoned by the fact that technical applications in general deal with thermally thick particles and that such an approach covers both reacting and shrinking core behaviour simultaneously.

2.4. Discrete Particle Method (DPM)

In order to predict the process of switchgrass combustion including heat-up, pyrolysis, combustion and emission formation, the Discrete Particle Method (DPM) was employed. Contrary to the continuum mechanics approach the Discrete Particle Method considers a packed bed of solid fuel as composed of discrete particles with individual shapes and sizes. Conversion processes are described by transient and one-dimensional conservation equations for mass and energy with sufficient accuracy. Chapman (1996) states that in general elaborate models are required to gain a deeper insight into the complexity of solid fuel conversion (Elliott, 1981; Laurendeau, 1978; Specht, 1983) as employed in the current study. The one-dimensional approach is supported by Man and Byeong (1994), whereas the transient character is emphasised by Lee et al. (1995; 1996). These requirements are met by the Discrete Particle Method, which offers a high degree of flexibility and detailed information. With the following assumptions
- one-dimensional and transient behaviour;
- intrinsic rate modelling;
- particle geometry represented by slab, cylinder or sphere;
- thermal equilibrium between gaseous, liquid and solid phases inside the particle the differential conservation equations for energy, gaseous and solid species Y_i describe particle conversion:

$$\frac{\partial(\upsilon c_p T)}{\partial t} = \frac{1}{r^n}\frac{\partial}{\partial r}\left(r^n \lambda_{eff}\frac{\partial T}{\partial r}\right) + \sum_{k=1}^{l}\dot{\omega}_k H_k \tag{11}$$

$$\frac{\partial Y_{i,gas}}{\partial t} = \frac{1}{r^n}\frac{\partial}{\partial r}\left(r^n D_i\frac{\partial Y_{i,gas}}{\partial r}\right) + \sum_{k=1}^{l}\dot{\omega}_{k,i,gas} \tag{12}$$

$$\frac{\partial Y_{i,solid}}{\partial t} = \sum_{k=1}^{l}\dot{\omega}_{k,i,solid} \tag{13}$$

where n defines the geometry of a slab ($n = 0$), cylinder ($n = 1$) or sphere ($n = 2$). The locally varying conductivity λ_{eff} is evaluated as Grønli (1996)

$$\lambda_{eff} = \varepsilon_p \lambda_g + \eta \lambda_{switchgrass} + (1-\eta)\lambda_c + \lambda_{rad} \tag{14}$$

which takes into account heat transfer by conduction in the gas, solid, char and radiation in the pore. The source term on the right hand side represents heat release or consumption due to chemical reactions. The conservation equations for gas and solid phase represent the time and spatially varying mass fractions of species Y_i including a reaction source term and diffusive transport for gas species. An effective diffusion coefficient $D_{i,eff} = D_i \varepsilon_p /\tau$ with ε_p and τ being porosity and tortuosity is employed to describe the diffusive transport (Dullien, 1979; Shih-I, 1977)

Reactions 7 and 8 are employed to describe the formation of sulphur dioxide for which the reaction rate terms are approximated by an Arrhenius expression of the following form:

$$\frac{dc_{SO2}}{dt} = k_1 e^{-Ea,1/RT} c_S c_{O2} \qquad (15)$$

$$\frac{dc_{SO2}}{dt} = k_2 e^{-Ea,2/RT} c_{K2SO4} c_{SiO2} \qquad (16)$$

where k_i, $E_{a,i}$ and T stand for reaction rate coefficients, activation energies and the local temperature of switchgrass, respectively. Thus, the parameters k_i and $E_{a,i}$ are determined by the least square approach so that the error between the predicted and measured profiles is minimised.

2.5. Initial and boundary conditions

Switchgrass was ground to a +20/-80 mesh that yields a mean particle diameter of $d = 5.0 \cdot 10^{-5}$ m. Within the reactor the sample is heated by a radiative flux, which is estimated to $q''_{rad} = 2.0 \cdot 10^5$ W/m^2 for a temperature $T_{rad} = 1373$ K. Due to the shielding effect of the boat for the sample, only half of the radiation flux reaches the switchgrass. It is cooled additionally by a convective flux of the incoming helium-oxygen mixture of which the temperature in the vicinity of the sample was measured and is displayed in Figure 2. According to Kaume (2003) the Nusselt number, Nu, for heat transfer evaluates as

$$Nu = f Nu_{m,sphere} \qquad (17)$$

for a loosely packed switchgrass sample with f and $Nu_{m,sphere}$ being an empirical correlation $f = 1.0 + 1.5(1.0 - \varepsilon)$ and the mean Nusselt number for a spherical geometry, respectively. Under laminar conditions prevailing during the experiments the latter is defined by

$$Nu_{m,sphere} = 2.0 + 0.664 Re^{1/2} Pr^{1/3} \qquad (18)$$

where Re and Pr denote the Reynolds and Prandlt numbers ($Pr \sim 0.68$ (Hänel, 2004)), respectively. Similarly, a mass transfer is described by a Sherwood number $Sh_{m,sphere}$ (Schönbucher, 2002)

$$Sh_{m,sphere} = 2.0 + 0.664 Re^{1/2} Sc^{1/3} \qquad (19)$$

where Sc is the Schmidt number. The viscosity of the helium-oxygen mixture was evaluated by data given by Kaye and Laby (2002).

Summarising the previous section the following boundary conditions for mass and heat transfer of a particle are applied:

$$-\lambda_{eff} \left.\frac{\partial T}{\partial r}\right|_R = \alpha(T_R - T_\infty) + \dot{q}_{rad} \qquad (20)$$

$$-D_{i,eff} \left.\frac{\partial c_i}{\partial r}\right|_R = \beta_i(c_{i,R} - c_{i,\infty}) \qquad (21)$$

where T_∞, $c_{i,\infty}$, α and β denote ambient gas temperature, concentration of species i, heat and mass transfer coefficients, respectively. Additionally, a radiative heat flux $\dot{q}_{rad}$ emanating from reactor walls is taken into account. For a detailed description of the Discrete Particle Method the reader is referred to Peters (Peters, 2003; Peters and Raupenstrauch, 2009).

2.6. Evaluation of kinetic parameters

The solution for heat-up, pyrolysis and combustion of a switchgrass particle was obtained by the Discrete Particle Method. Pyrolysis was modelled by an approach of Miller and Bellan (1997) for organic matter, while combustion of charred material was represented by the model of Kulasekaran et al. (1998). It includes an intrinsic rate mechanism that approximates the combustion process with sufficient accuracy (Peters, 2003). The kinetics of the sulphur dioxide emission forming reactions 7 and 8 are described by an Arrhenius equation, which includes an activation energy $E_{a,i}$ and a pre-exponential factor k_i. For a given set of kinetic parameters and in conjunction with mass transfer and heat transfer due to convection and radiation the spatial and time dependent temperature and species distribution within the particle was obtained by the Discrete Particle Method. The profiles of sulphur dioxide were compared to experimental data and the kinetic parameters were subsequently corrected by the least square method so that the deviation between the measurements and predictions was minimised as shown in Figure 4.
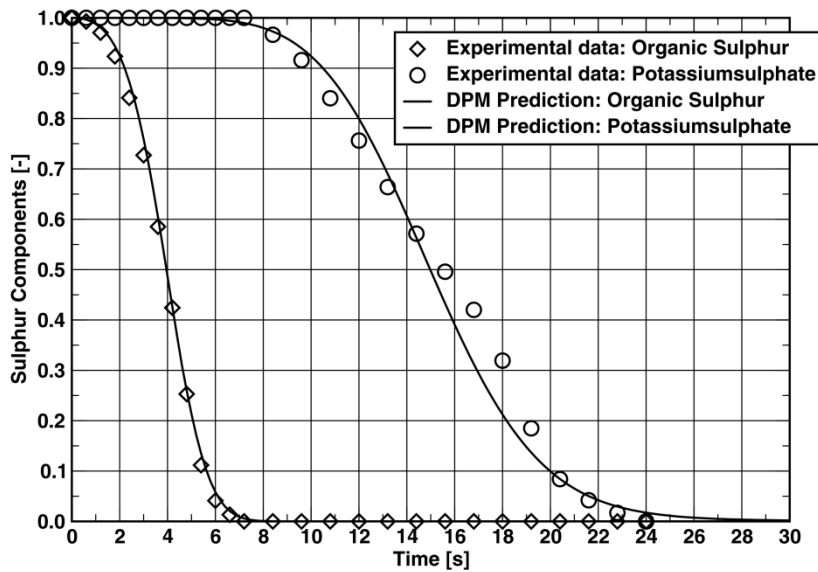

Fig. 4. Conversion of organic sulphur and potassium sulphate during combustion of switchgrass

A comparison between the measured data and predictions shows good agreement for both the distribution and the period needed to form sulphur dioxide. The values for the activation energy and pre-exponential factor describing the reaction rate are listed in Eqs. 22 and 23.

$$\frac{dc_{SO2}}{dt} = 7.29 \cdot 10^5 e^{-59500.0/RT} c_S c_{O2} \tag{22}$$

$$\frac{dc_{SO2}}{dt} = 1.21 \cdot 10^5 e^{-130000.0/RT} c_{K2SO4} c_{SiO2} \tag{23}$$

The corresponding surface temperature of the switchgrass particle is shown in Figure 5. The experimental data corresponds to the ambient temperature measured in the vicinity of the sample.

During the first stage of the process a rapid increase of the temperature on the switchgrass surface occurs as an effect of the radiative heat flux. The heat transfer due to convection is described with the empirical relationship of Eq. 17 assuming that the gas temperature contributes to the convective flux between the particle and the gas. Thus, as seen in Figure 5, the temperature profiles of the surface and those of the gas are compatible. These is, however, a shift varying between ~300 K and ~400 K during the conversion process.
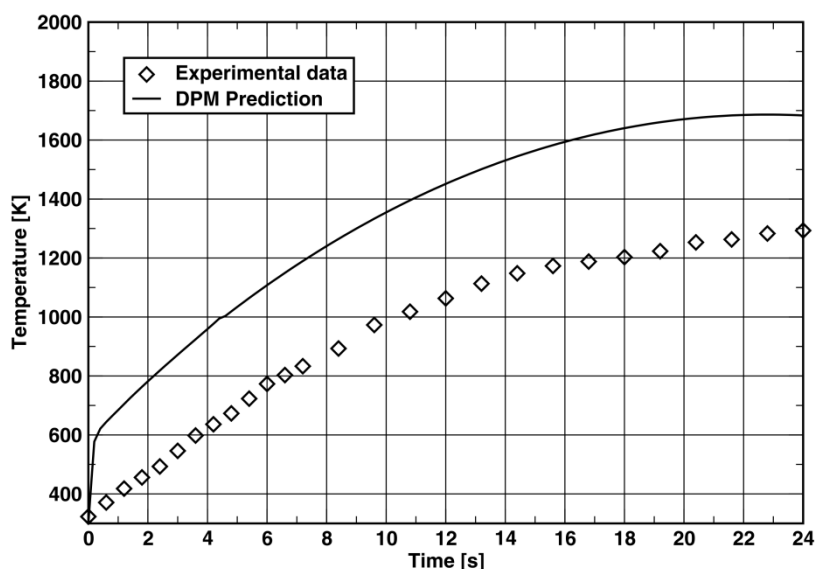
Fig. 5. Temperature of a switchgrass particle during combustion and gas temperature measured in its vicinity

3. RESULTS AND DISCUSSION

Since the results of the previous section refer to almost pulverised switchgrass samples, the studies within the following section address predictions of raw material emissions as harvested and delivered for combustion.

3.1. Influence of blade geometry

Thus, further investigations into sulphur dioxide formation concern particle shape and size. The cylindrical geometry describes blades of grass more properly than spherical one. Thus, the conservation equations for mass and energy are solved in a cylindrical system. In order to examine the impact of geometry on the solution, the radius is kept constant for which the results are presented in Figure 6.
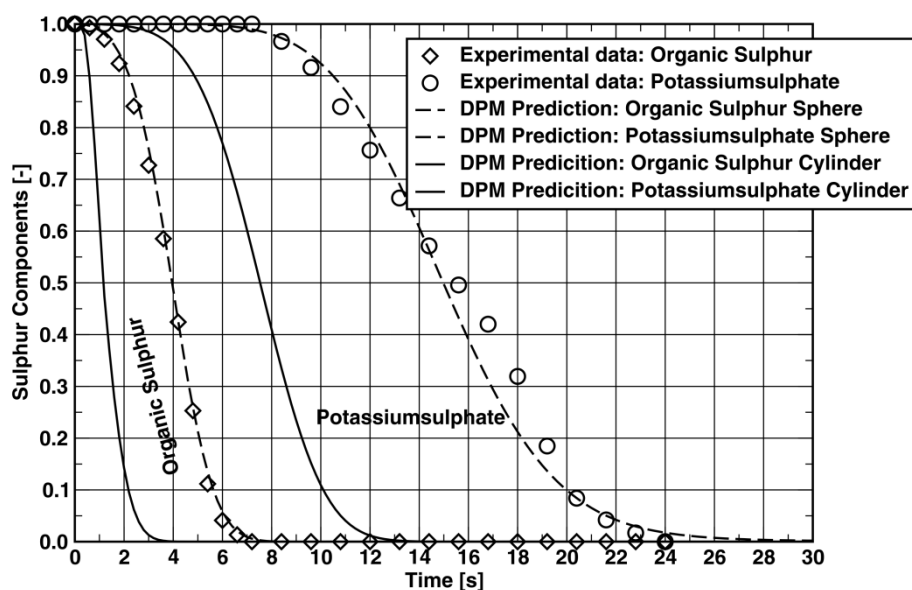

Fig. 6. Decrease of organic sulphur and potassium sulphate (dimensionless) in a cylindrical and spherical particle during combustion of switchgrass

A faster sulphur dioxide formation is predicted for a cylindrical geometry with formation periods shortened by ~6 s and ~10 s for organic sulphur and potassium sulphate, respectively. Since the surface to volume ratio of a cylinder is bigger than that of a sphere, a cylinder offers a larger surface for heat transfer. It generates a higher heating rate as depicted in Figure 7, and thus, increases the formation rate of sulphur dioxide.
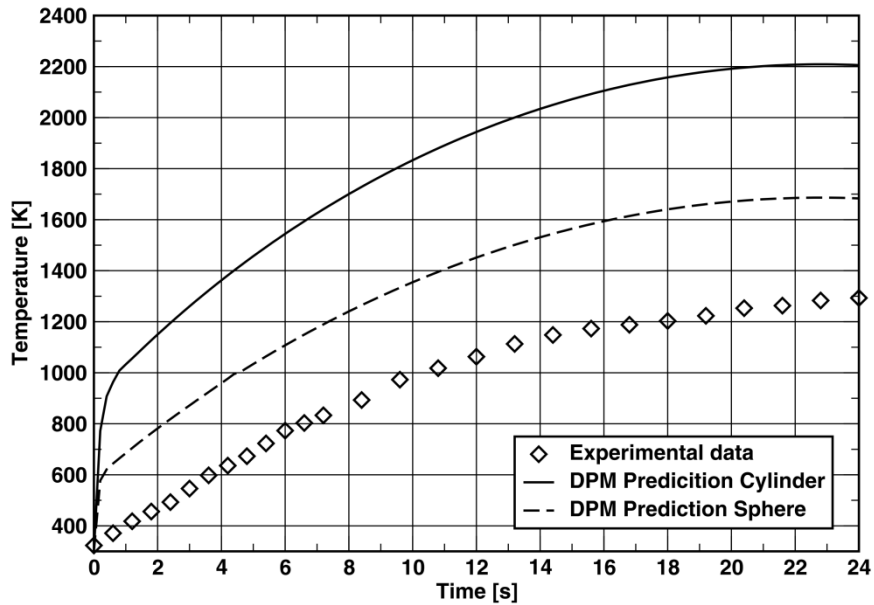
Fig. 7. Temperature of a cylindrical and spherical switchgrass particle during combustion

3.2. Influence of blade size

In order to account for different sizes of switchgrass the radius was varied between $r_1 = 1\,\text{mm}$ and $r_2 = 5\,\text{mm}$, which is assumed to cover the range of harvested switchgrass. The impact on the formation time under furnace relevant heat transfer rates of $\dot{q}'' = 20.0\,\text{kW/m}^2$ is presented in Figure 8.
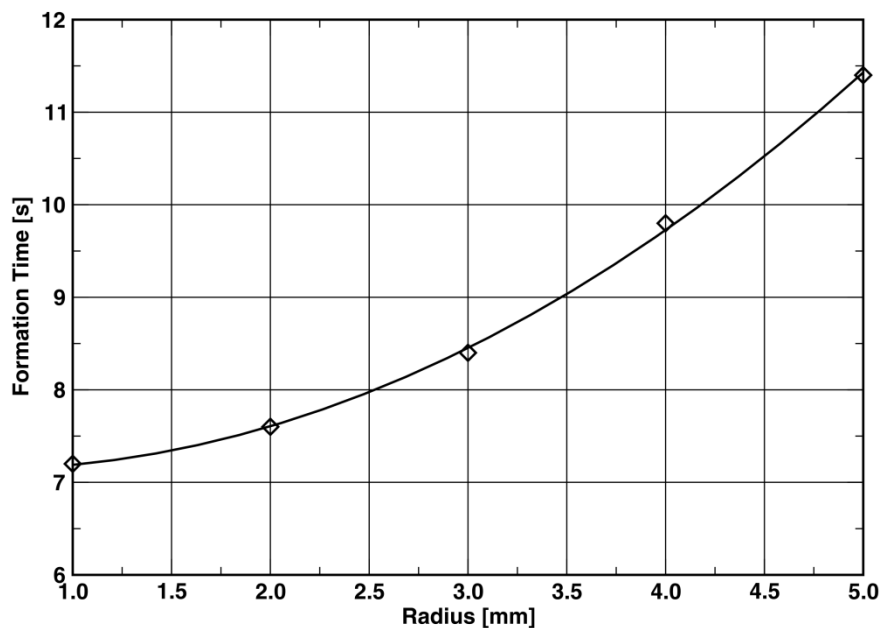
Fig. 8. Time of formation of sulphur-dioxide depending on the radius for a cylindrical shape

The result in Figure 8 indicates that the period of complete formation increases by ~40% while the size of switchgrass blades increases by   . Compared to thermally thin particles, as depicted in Figure 6, larger particles experience significant spatial gradients. Hence, larger blades undergo much more prolonged combustion period, and thus, higher temperatures evolve inside a blade as shown in Figure 9.
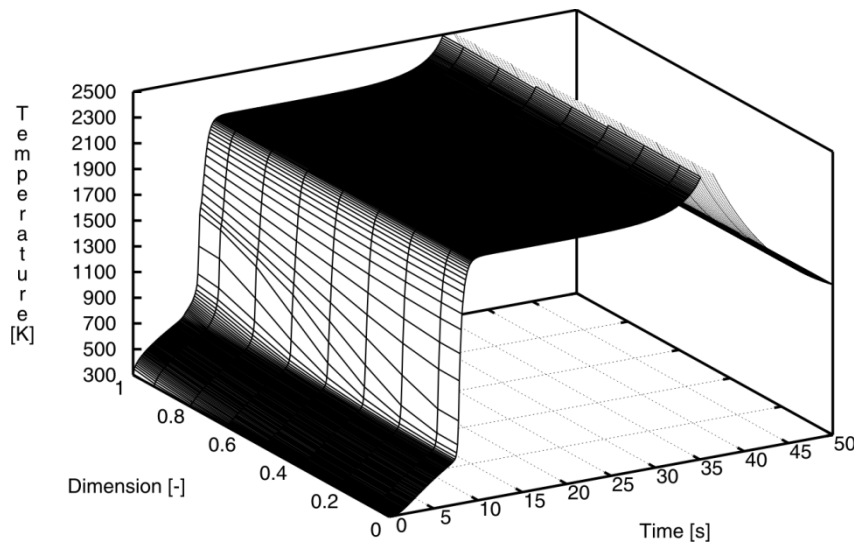

Fig. 9. Temperature profile for a cylindrical switchgrass blade of 5 mm in radius

Once, the blade has reached ignition conditions it enters a period of steady-state combustion with temperatures of ~2150 K as compared to temperatures of ~1700 K for the ground sample. Towards the end of the combustion period at a time of ~35 s the remaining ash of the switchgrass undergoes heat transfer only resulting in decreasing the temperature.

Although the spatial temperature is rather uniform during the combustion period, the distribution of oxygen experiences large gradients versus radius of the switchgrass blades as shown in Figures 10 and 11.
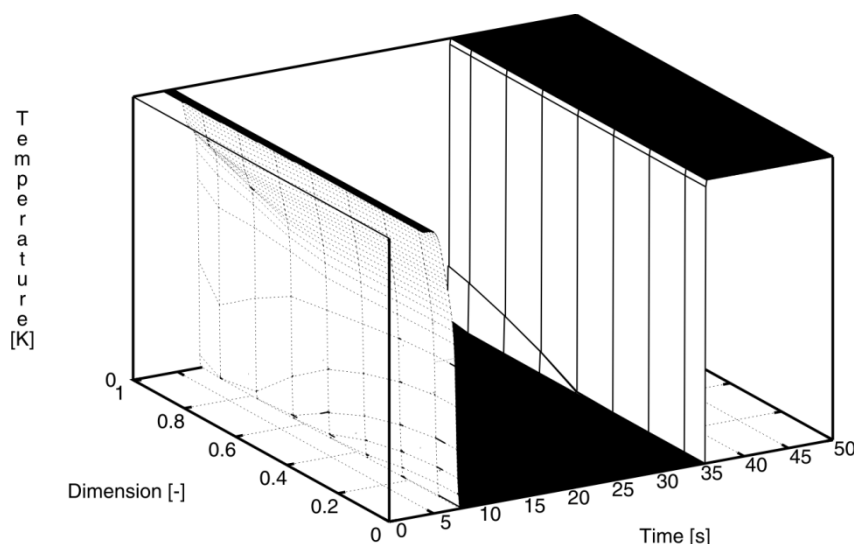

Fig. 10. Oxygen profile for a cylindrical switchgrass blade of 5 mm in radius

In particular, Figure 11 depicts strong gradients of oxygen between the surface and half the radius inside the blade over an enlarged period during combustion, and thus, indicating that the reaction process is limited by transport of available oxygen. Contrary to lumped parameter models, the Discrete

Particles Method resolves spatial gradients, and therefore is equally well applicable to reacting and shrinking core modes of combustion that a particle most probably undergoes during a transition.
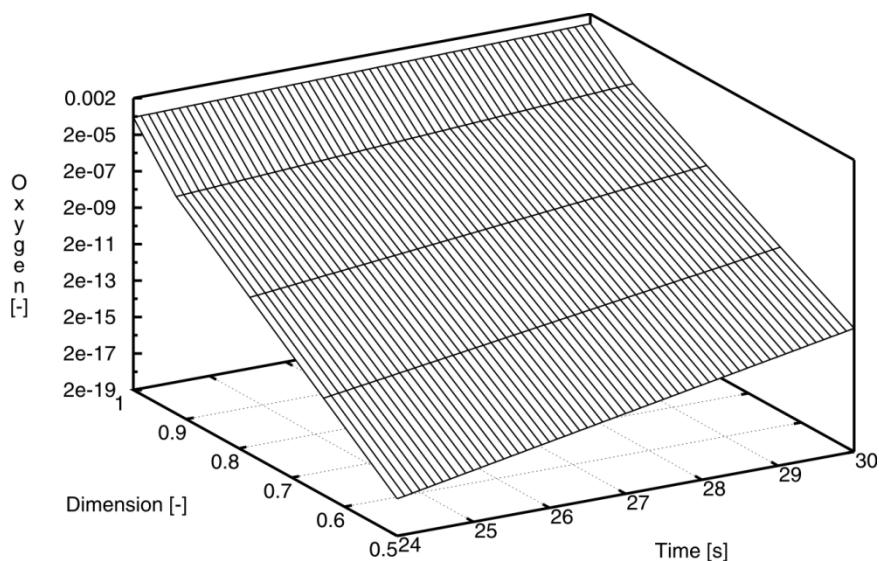

Fig. 11. Enlarged oxygen profile for a cylindrical switchgrass blade of 5 mm in radius

3.3. Correlation between formation of sulphur dioxide and depletion of organic matrix

Undoubtedly the formation of any kind of emission is strongly coupled to the overall conversion of organic material. During thermal conversion of switchgrass its organic matrix is first converted to charred material during pyrolysis. Since a part of available sulphur is bound to the organic matrix depletion of organically bound sulphur is correlated to the conversion of the organic matrix as shown in Figure 12.
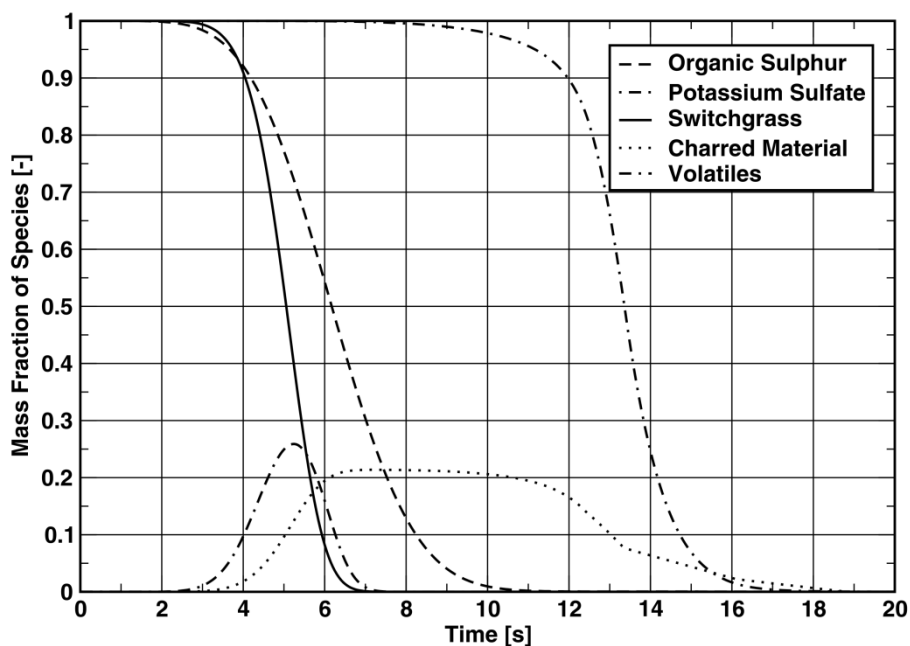

Fig. 12. Correlation between emission formation and depletion of organic matrix

The prediction illustrates that ~80% of organically bound sulphur reacts during the period of pyrolysis. Similarly, inorganically bound sulphur reacts mainly during the conversion period of charred material.

Predicted results in Figure 12 suggest that the start and end of depletion of potassium sulphate correlates very well with the combustion period of charred material.

4. SUMMARY

The formation of sulphur dioxide during combustion of a switchgrass was investigated and compared to experimental data presented by Dayton et al. (1995). Formation of sulphur dioxide was modelled by two reactions, namely an oxidation of sulphur bound in an organic matrix and a reaction between potassium sulphate and silicon dioxide. The Arrhenius-like approach was employed to describe the kinetics of the reactions. Kinetic parameters, i.e. an activation energy and pre-exponential factor were determined by the least-square method so that the deviation between the measured and predicted profile was minimised.

A simulation of switchgrass conversion including heating-up, pyrolysis and combustion was modelled by the Discrete-Particle-Method (DPM). This method represents a transient and one-dimensional approach for solving the differential conservation equations of mass and energy. Thus, in conjunction with the initial and boundary conditions and a given set of kinetic parameters sulphur dioxide emission was predicted. Good agreement between the measurements and predictions was achieved. An error analysis showed that an upper standard error of 14 % was not exceeded.

REFERENCES

Aho M., Silvennoinen J, 2004. Preventing chlorine deposition on heat transfer surfaces with aluminium-silicon rich biomass residue and additive. *Fuel*, 83, 1299–1305. DOI: 10.1016/j.fuel.2004.01.011.

Aho M., Ferrer E., 2005. Importance of coal ash composition in protecting the boiler against chlorine deposition during combustion of chlorine-rich biomass. *Fuel*, 84, 201–212. DOI: 10.1016/j.fuel.2004.08.022.

Chapman P., 1996. CFD enhances waste combustion design and modification. *Combustion Canada `96*. Ottawa, Ontario, Canada.

Dayton D.C., French R.J., Milne T.A., 1995. Direct observation of alkali vapor release during biomass combustion and gasification. 1. Application of molecular beam/mass spectrometry to switchgrass combustion. *Energy Fuels*, 9, 855–865. DOI: 10.1021/ef00053a018.

Dullien F.A.L., 1979. *Porous media fluid transport and pore structure*. San Diego, Academic Press.

Elliott M.A., 1981. *Chemistry of coal utilization*. Wiley, New York.

Ericsson K., 2007. Co-firing — A strategy for bioenergy in Poland? *Energy*, 32, 1838–1847. DOI: 10.1016/j.energy.2007.03.011.

Grønli M., 1996. *A theoretical and experimental study of the thermal degradation of biomass*. NTNU, Trondheim.

Hänel D., 2004. *Molekulare Gasdynamik.* Springer-Verlag, Berlin, Heidelberg.

Kaume M., 2003. *Transportvorgänge in Der Verfahrenstechnik.* Springer. Berlin, Germany.

Kaye G.W.C., Laby T.H., 2002. *Handbook of Physics*. Springer, New York.

Knudsen J.N., Jensen P.A., Dam-Johansen K.. 2004a. Transformation and release to the gas phase of Cl, K, and S during combustion of annual biomass. *Energy Fuels*, 18, 1385–1399. DOI: 10.1021/ef049944q.

Knudsen J.N., Jensen P.A., Lin W., Dam-Johansen K., 2005. Secondary capture of chlorine and sulfur during thermal conversion of biomass. *Energy Fuels*, 19, 606–617. DOI: 10.1021/ef049874n.

Knudsen J.N., Jensen P.A., Lin W., Frandsen F.J., Dam-Johansen K., 2004b. Sulfur transformation during thermal conversion of herbaceous biomass. *Energy Fuels*, 18, 810–819. DOI: 10.1021/ef034085b.

Koyuncu T., Pinar Y., 2007. The emissions from a space-heating biomass stove. *Biomass Bioenergy*, 31, 73–79. DOI: 10.1016/j.biombioe.2006.06.014.

Kulah G., 2010. Validation of a FBC model for co-firing of hazelnut shell with lignite against experimental data. *Exp. Therm. Fluid Sci.*, 34, 646–655. DOI: 10.1016/j.expthermflusci.2009.12.006.

Kulasekaran S., Linjewile T.M., Agarwal P.K., Biggs M.J., 1998. Combustion of porous char particle in an incipiently fluidized bed. *Fuel*, 77, 1549–1560. DOI: 10.1016/S0016-2361(98)00091-X.

Langn T., Jensen P.A., Knudsen J.N., 2006. The effects of Ca-based sorbents on sulfur retention in bottom ash from grate-fired annual biomass. *Energy Fuels*, 20, 796–806. DOI: 10.1021/ef050243i.

Laurendeau N.M., 1978. Heterogeneous kinetics of coal char gasification and combustion. *Prog. Energy Combust. Sci.*, 4, 221–270. DOI: 10.1016/0360-1285(78)90008-4.

Lee J.C., Yetter R.A., Dryer F.L., 1995. Transient numerical modelling of carbon ignition and oxidation. *Combust. Flame*, 101, 387–398. DOI: 10.1016/0010-2180(94)00207-9.

Lee J.C., Yetter R.A., Dryer F.L., 1996. Numerical simulation of laser ignition of an isolated carbon particle in quiescent environment. *Combust. Flame*, 105, 591–599. DOI: 10.1016/0010-2180(96)00221-0.

Man Y.H., Byeong R., 1994. A numerical study on the combustion of a single carbon particle entrained in a steady flow. *Combust. Flame*, 97, 1–16. DOI: 10.1016/0010-2180(94)90112-0.

Matsuda H., Ozawa S., Naruse K., Ito K., Kojima Y., Yanase T., 2005. Kinetics of HCl emission from inorganic chlorides in simulated municipal wastes incineration conditions. *Chem. Eng. Sci.*, 60, 545–552. DOI: 10.1016/j.ces.2004.07.13110.1016/j.ces.2004.07.131.

McLaughlin S., Bouton J., Bransby D., Conger B., Ocumpaugh W., Parrish D., Taliaferro C., Vogel K., Wullschleger S., 1999. Developing switchgrass as a bioenergy crop, In: Janick J. (Ed.) *Perspectives on new crops and new uses*, 282–299. ASHS Press, Alexandria, VA.

Michelsen H.P., Frandsen F., Dam-Johansen K., Larsen O.H., 1998. Deposition and high temperature corrosion in a 10 MW straw fired boiler. *Fuel Process. Technol.*, 54, 95–108. DOI: 10.1016/S0378-3820(97)00062-3.

Miller R.S., Bellan J., 1997. A generalized biomass pyrolysis model based on superimposed cellulose, hemicellulose and lignin kinetics. *Combust. Sci. Technol.*, 126, 97–137. DOI: 10.1080/00102209708935670.

Miranda T., Román S., Montero I., Nogales-Delgado S., Arranz J.I., Rojas C.V., González J.F., 2012. Study of the emissions and kinetic parameters during combustion of grape pomace: Dilution as an effective way to reduce pollution. *Fuel Process. Technol.*, 103, 160–165. DOI: 10.1016/j.fuproc.2011.10.002.

Misra M.K., Ragland K.W., Baker A.J., 1993. Wood ash composition as a function of furnace temperature. *Biomass Bioenergy*, 4, 103–116. DOI: 10.1016/0961-9534(93)90032-Y.

Nielsen H.P., Frandsen F.J., Dam-Johansen K., Baxter L.L., 2000. The implications of chlorine-associated corrosion on the operation of biomass-fired boilers. *Progress Energy Combust. Sci.*, 26, 283–298. DOI: 10.1016/S0360-1285(00)00003-4.

Peters B., 1999. Classification of combustion regimes in a packed bed of particles based on relevant time and length scales. *Combust. Flame*, 116, 297–301. DOI: 10.1016/S0010-2180(98)00048-0.

Peters B., 2003. *Thermal conversion of solid fuels*. WIT Press, Southampton.

Peters B., Raupenstrauch H., 2009. Modelling moving and fixed bed combustion, In: Winter F., Lackner M., Agarwal A. (Eds.) *Combustion Handbook*. Wiley.

Roy M.M., Corscadden K.W., 2012. An experimental study of combustion and emissions of biomass briquettes in a domestic wood stove. *Applied Energy*, 99, 206–212. DOI: 10.1016/j.apenergy.2012.05.003.

Schönbucher A., 2002. *Thermische Verfahrenstechnik*. Springer.

Shih-I P., 1977. *Two-Phase Flows*. Vieweg Tracts in Pure and Applied Physics, Braunschweig.

Specht E., 1993. *Kinetik Der Abbaureaktionen*. TU Clausthal-Zellerfeld.

VanLith S.C., Alonso-Ramirez V., Jensen P.A., Frandsen F.J., Glarborg P., 2006. Release to the gas phase of inorganic elements during wood combustion. Part 1: Development and evaluation of quantification methods. *Energy Fuels*, 20, 964–978. DOI: 10.1021/ef050131r.

Verma V.K., Bram S., Gauthier G., De Ruyck J., 2011. Performance of a domestic pellet boiler as a function of operational loads: Part-2. *Biomass Bioenergy*, 35, 272–279. DOI: 10.1016/j.biombioe.2010.08.043.

Wiinikka H., Gebart R., Boman C., Bostrom D., Öhman M., 2007. Influence of fuel ash composition on high temperature aerosol formation in fixed bed combustion of woody biomass pellets. *Fuel*, 86, 181–193. DOI: 10.1016/j.fuel.2006.07.001.

Zheng Y., Jensen P.A., Sander B., Junker H., 2007. Ash transformation during co-firing coal and straw. *Fuel*, 86, 1008–1020. DOI: 10.1016/j.fuel.2006.10.008.

Ściążko M., Zuwała J., Pronobis M., Winnicka G., 2007. *Problemy Zwiazane Ze Wspolpalaniem Biomasy w Kotlach Energetycznych*. Instytut Chemicznej Przeróbki Węgla, Politechnika Śląska, Zabrze, Poland (in Polish).

APPENDIX: ERROR ESTIMATION

The accuracy of the predicted results and particularly the kinetic parameters as pre-exponatial factors and activation energies are addressed in the following section. Due to a lack of radiative material properties of the interior part of the reactor the sensitivity of the radiative flux on the kinetic parameters was investigated. A given reactor temperature of $T_R \sim 1372$ K would evaluate to a maximum specific radiative heat flux of $\dot{q}'' \sim 100000$ W/m^2 including the shielding effect of the boat by a factor of 0.5. However, radiative material properties reduce the above-mentioned flux, so that half the values were taken as the lower bound. The rate of formation was predicted under these conditions and the results are shown in Figure 13.
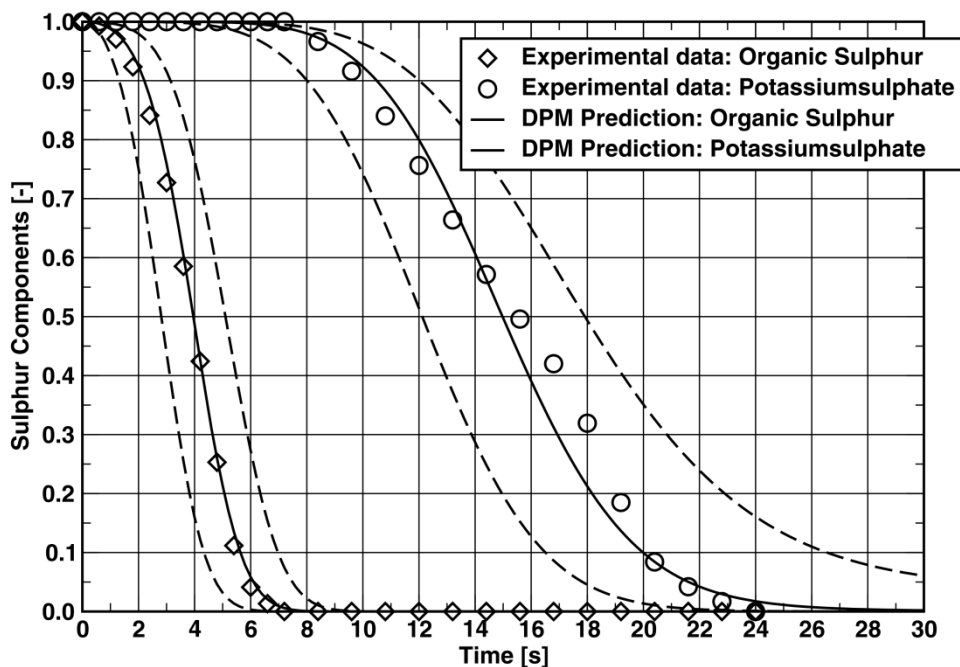

Fig. 13. Influence of heat transfer on evaporation of sulphur dioxide release

It leads to the following expressions of the reaction rates:

$$\frac{dc_{SO2}}{dt} = 3.83 \cdot 10^5 \, e^{-48903.0/RT} c_S c_{O2} \quad \text{for} \quad \dot{q}'' \sim 50000 \, \text{W/m}^2 \tag{A-1}$$

$$\frac{dc_{SO2}}{dt} = 1.11 \cdot 10^5 \, e^{-119925.0/RT} c_{K2SO4} c_{SiO2} \quad \text{for} \quad \dot{q}'' \sim 50000 \, \text{W/m}^2 \tag{A-2}$$

$$\frac{dc_{SO2}}{dt} = 1.21 \cdot 10^6 \, e^{-69997.0/RT} c_S c_{O2} \quad \text{for} \quad \dot{q}'' \sim 100000 \, \text{W/m}^2 \tag{A-3}$$

$$\frac{dc_{SO2}}{dt} = 5,52 \cdot 10^5 \, e^{-161132.0/RT} c_{K2SO4} c_{SiO2} \quad \text{for} \quad \dot{q}'' \sim 100000 \, \text{W/m}^2 \tag{A-4}$$

Although the radiative heat transfer varies by a factor of ~2 the standard error evaluated by

$$S.E. = \sqrt{\frac{\sum \Delta y^2}{n}} \qquad \text{(A-5)}$$

amounts to 9% and 14% for the upper and lower bounding curve in Figure 13, respectively. Therefore, the kinetic parameters between the upper and lower bounding curve are assumed to fit best the kinetics of sulphur dioxide formation.